Structures 88 (2026) 111865

Contents lists available at ScienceDirect

Structures

journal homepage: www.elsevier.com/locate/structures

Global isolation period for rigid nonstructural components

Juan Carlos Obando [a,*], Diego Lopez-Garcia [b], Orlando Arroyo [c], Daniela Novoa [d], Henry A. Colorado [e]

[a] Environmental School, Universidad de Antioquia UdeA, Calle 70 No. 52-21, Medellín, Colombia
[b] Department of Structural & Geotechnical Engineering, Pontificia Universidad Catolica de Chile, Avda. Vicuña Mackenna 4860 Macul, Santiago, Chile
[c] Universidad Industrial de Santander, Bucaramanga, Colombia
[d] EstrucMed Ingeniería especializada S.A.S., Carrera 43A No. 7-50, Medellín, Colombia
[e] CCComposites Laboratory, Universidad de Antioquia UdeA, Calle 70 No. 52-21, Medellín, Colombia

ARTICLE INFO

Keywords:
Floor accelerations
Global isolation period
Nonstructural components
Nonstructural elements
Seismic design
Seismic isolation

ABSTRACT

Non-Structural Components (NSCs) comprise all building elements that are not part of the load-bearing system. These elements are often subjected to floor accelerations significantly higher than ground accelerations, which can compromise building functionality and are generally the primary source of post-earthquake losses. A potential strategy to mitigate these demands is to equip NSCs with seismic isolation systems. However, few studies have attempted to generalize the seismic behavior of isolated NSCs. This study introduces the concept of the global isolation period (T_g), defined as the period of a seismic isolation device for rigid NSCs that ensures a target reduction in acceleration demands, regardless of the NSC's location within the building or the damping ratio adopted for the isolation system. To establish T_g, an extensive parametric study is conducted on the response of rigid NSCs isolated and anchored at different levels of various elastic buildings. Based on this analysis, a simple equation is proposed that relates T_g to the fundamental period of the building and the target reduction in NSC accelerations. The equation is validated using accelerations obtained from three inelastic reinforced concrete frame buildings, considering the Friction Pendulum System (FPS) as the isolation device for the NSCs. The proposed equation for T_g provides reasonable estimates that can serve as a basis for the design of seismic isolation devices for NSCs. It yields conservative results when the target acceleration reduction of the rigid NSC is close to 50%, whereas for larger reductions it tends to be less conservative.

1. Introduction

Non-Structural Components (NSCs) are all the elements present in buildings that do not form part of the load-resisting system. Examples of NSCs include mechanical and electrical equipment, partition walls, parapets, pipes, ducts, and contents, among others. Although NSCs are not part of the structural system, they are also exposed to seismic actions and play a fundamental role in the seismic performance of buildings. Inadequate seismic design of these components may compromise the operability of buildings even if the structural system remains undamaged after an earthquake. Instances of such impacts have been observed in recent major earthquakes, such as those in Turkey (2023), Chile (2010), New Zealand (2010 and 2011), and Ecuador (2016) [11,27,28,45].

Moreover, NSCs typically account for between 70% and 85% of the total cost in residential and office buildings, and up to 90% in critical facilities such as hospitals [51]. This implies that most economic losses after an earthquake correspond to these elements. Furthermore, traditional seismic design methods for buildings do not allow for accurate determination of the seismic demands of NSCs. For this reason, over the past decades, the study of the seismic behavior of NSCs has been the subject of numerous research works [10,13,2,20,21,3,30,35–38,42,50,6].

From a seismic design perspective, NSCs can be classified into two broad groups: acceleration-sensitive and displacement-sensitive. The first group includes those whose seismic demand is governed by the peak absolute acceleration at their anchorage points, such as mechanical and electrical equipment, parapets, ducts, and pipes. Since these components are mainly located at different floors within the building, they are exposed to seismic accelerations with characteristics that differ from

* Corresponding author.
E-mail addresses: jcarlos.obando@udea.edu.co (J.C. Obando), dlg@uc.cl (D. Lopez-Garcia), odarrame@uis.edu.co (O. Arroyo), danielanora@unisabana.edu.co (D. Novoa), henry.colorado@udea.edu.co (H.A. Colorado).

https://doi.org/10.1016/j.istruc.2026.111865
Received 19 September 2025; Received in revised form 23 December 2025; Accepted 11 April 2026
Available online 17 April 2026
2352-0124/© 2026 The Authors. Published by Elsevier Ltd on behalf of Institution of Structural Engineers. This is an open access article under the CC BY-NC-ND license (http://creativecommons.org/licenses/by-nc-nd/4.0/).

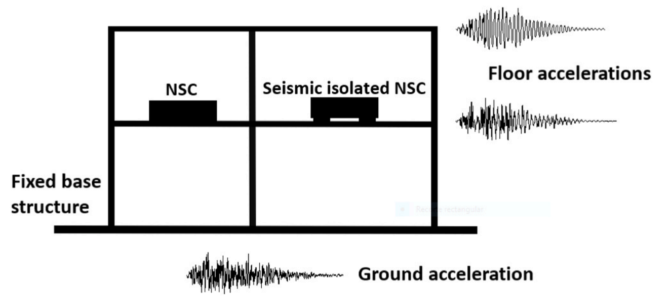

Fig. 1. Differences between ground and floor accelerations and Nonstructural Components (NSCs) with and without isolation systems.

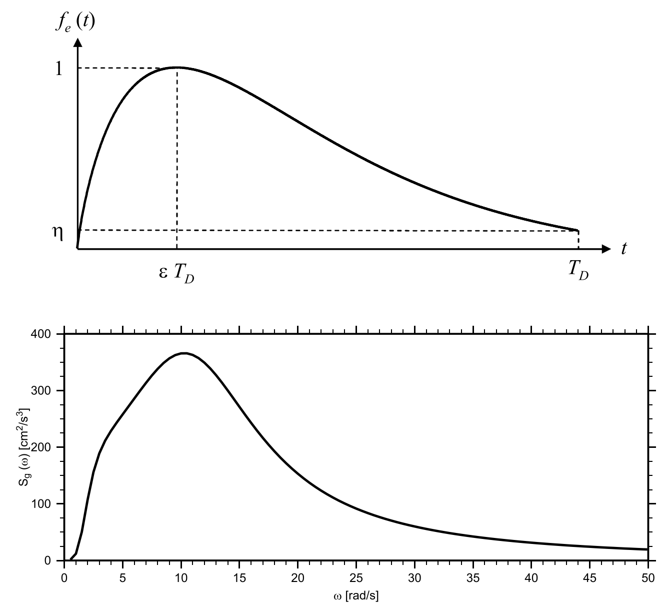

Fig. 2. Modulating function $f_e(t)$ and Modified Kanai-Tajimi power spectral density function S_g ($\omega_g = 12.50$ rad/s, $\xi_g = 0.60$, $\omega_f = 2.00$ rad/s, $\xi_f = 0.70$ and $S_O = 200$ cm^2/s^3).

those experienced at ground level. This occurs because the building acts as a filter and amplifier of ground accelerations before they reach each floor (Fig. 1). For instance, peak floor accelerations (PFAs) can easily reach values two to three times higher than those recorded at the ground [1,14,18,19,24,37,44,47].

One alternative to significantly reduce the absolute acceleration demands on NSCs is to equip them with seismic isolation systems. These systems have been shown to effectively reduce building and bridge accelerations [8,23,52]. However, in certain cases, this solution may prove unfeasible due to its high cost, the clearance required between buildings, restrictions imposed during retrofitting processes [5], or the need to isolate only specific components. For these reasons, seismic isolation systems that can be applied directly to NSCs have been proposed. Fig. 1 illustrates this concept schematically. Examples of these systems include those described by Mo et al. [33,34], Reggio and De Angelis [43], Liu and Warn [25], Gavin and Zaicenco [15], Khechfe et al. [22], Ismail et al. [17] and Meng et al. [32]. However, these studies have examined specific cases, such as when the NSC is connected to one type of structural system [25] or when the NSC is subjected only to ground accelerations [32] or when non-traditional isolation devices are used [15,17,26,33,34]. To date, no studies have generalized the seismic behavior of isolated NSCs. Consequently, there is still no methodology that enables engineers to readily estimate the design period required for NSC isolation systems based on the supporting building's dynamic properties and the desired reduction in seismic demand.

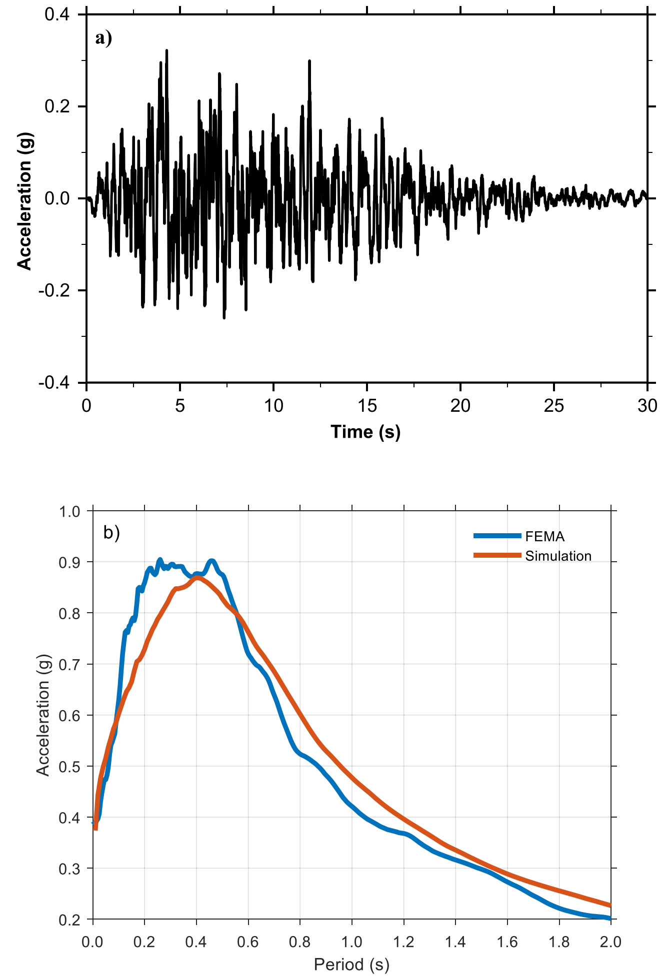

Fig. 3. a) Sample realization $\ddot{u}_g(t)$ of the ground acceleration process $\ddot{U}_g(t)$; b) Average response spectra of FEMA P695 and simulated ground motions.

This study addresses this gap and introduces the concept of a global isolation period (T_g) for rigid NSCs. This period is defined as the minimum isolation period required to guarantee a target reduction in acceleration demands, regardless of the NSC's location within the building and the damping ratio of the isolation system. To this end, a comprehensive parametric study is carried out on the response of isolated rigid NSCs anchored at different levels of various elastic buildings. Seismic excitations are generated through Monte Carlo simulations, and a linear isolation system is adopted for the NSCs. Finally, a simple equation is proposed to relate the global isolation period with the fundamental period of the building and with the target reduction in peak absolute acceleration demands of the NSCs. The equation is validated using accelerations obtained from three real reinforced concrete frame buildings (RCFBs) and considering the Friction Pendulum System (FPS) as the seismic isolation device for the NSCs.

2. Seismic excitations and buildings used to develop the global isolation period equation

The ground acceleration used for the development of the equation for the global isolation period is modeled as a Gaussian, zero-mean nonstationary random process $\ddot{U}_g$ *(t)* whose evolutionary power spectral density function $S_{\ddot{U}g}$ *(t, ω)* is given by:

$$S_{\ddot{U}g}(t,\omega) = [f_e(t)]^2 S_g(\omega) \tag{1}$$

where t denotes time, ω indicates circular frequency, $f_e(t)$ is a

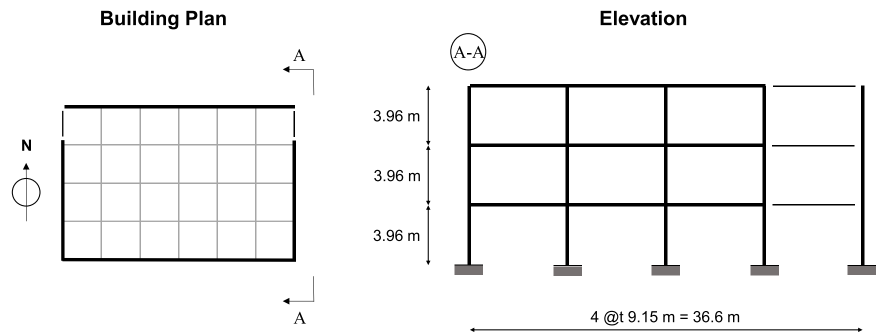

Fig. 4. Description of the 3-story steel building [40].

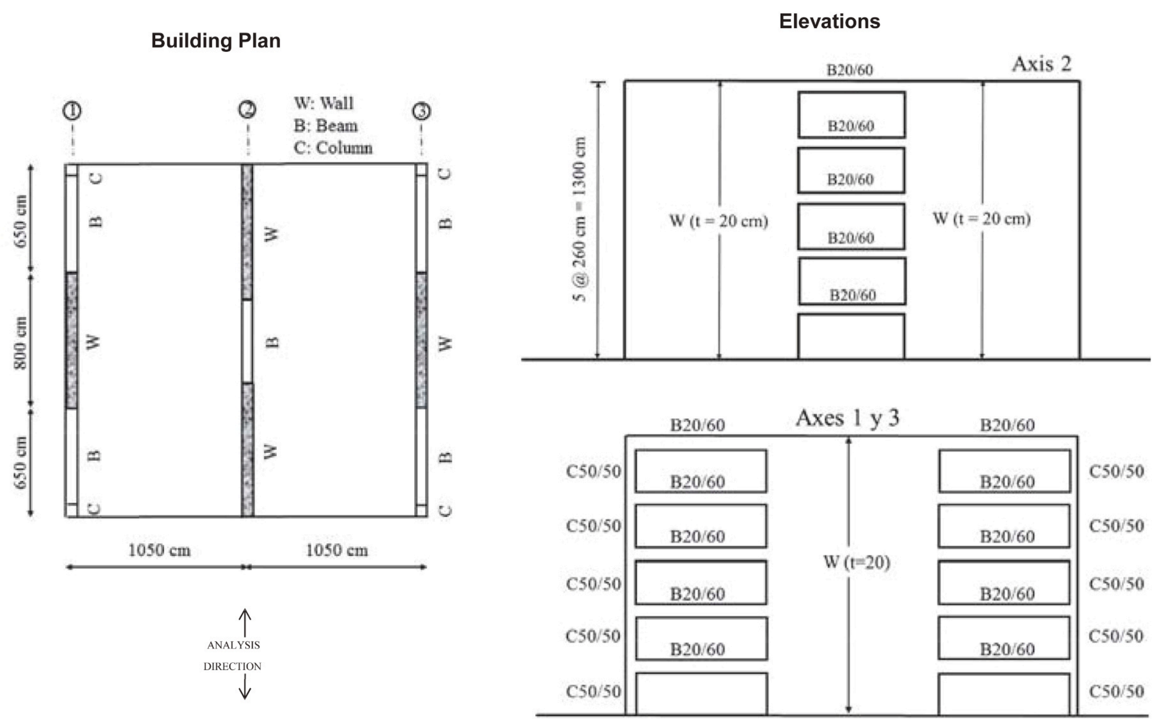

Fig. 5. Description of the 5-story RC wall building [49].

modulating (sometimes also referred to as "envelope" or "window") time function and $S_g(\omega)$ is a stationary power spectral density function. The modulating function $f_e(t)$ is assumed equal to that initially proposed by Saragoni and Hart [46] and calibrated later by Boore [4], which is given by:

$$f_e(t) = at^b e^{-ct} \tag{2}$$

where:

$$a = \left(\frac{e}{\varepsilon T_D}\right)^b \tag{3}$$

$$b = -\frac{\varepsilon \ln(\eta)}{1 + \varepsilon[\ln(\varepsilon - 1)]} \tag{4}$$

$$c = \frac{b}{\varepsilon T_D} \tag{5}$$

where, in turn, T_D is the duration of the excitation and η and ε are constants that define the shape of $f_e(t)$ (Fig. 2). In this study, constant T_D is set equal to 30 s. Based on what is recommended in Boore [4], constants η and ε are set equal to 0.05 and 0.20, respectively. The power spectral density function $S_g(\omega)$ is assumed equal to that defined by the modified Kanai-Tajimi function (sometimes also referred to as the Clough-Penzien function), which is given by [9]:

$$S_g(\omega) = \left[\frac{\omega_g^4 + 4\xi_g^2\omega_g^2\omega^2}{\left(\omega_g^2 - \omega^2\right)^2 + 4\xi_g^2\omega_g^2\omega^2}\right]\left[\frac{\omega^4}{\left(\omega_f^2 - \omega^2\right)^2 + 4\xi_f^2\omega_f^2\omega^2}\right]S_0 \tag{6}$$

In this study, constants ω_g, ξ_g, ω_f, ξ_f and S_0 are set equal to 12.50 rad/s, 0.60, 2.00 rad/s, 0.70 and $S_0 = 200$ cm^2/s^3, respectively. The resulting power spectral density function $S_g(\omega)$ is shown in Fig. 2. The corresponding main frequency ω_m (i.e., the frequency at which $S_g(\omega)$ takes its maximum value) is equal to 10.26 rad/s, and the period T_m associated with the main frequency is equal to $(2\pi)/10.26$ rad/s = 0.60 s. For illustration purposes, a sample realization $\ddot{u}_g(t)$ of the resulting seismic excitation process $\ddot{U}_g(t)$, generated through standard simulation techniques [48], is shown in Fig. 3a,

In addition, Fig. 3b shows the average response spectra of two groups of seismic records: a) those obtained with Monte Carlo simulation and b) those obtained using a set of actual far-field seismic accelerations recorded on firm soil conditions (FEMA P-695). Fig. 3b shows that the two groups of seismic records have similar frequency content. In this study, far-field accelerations are prioritized because most of the

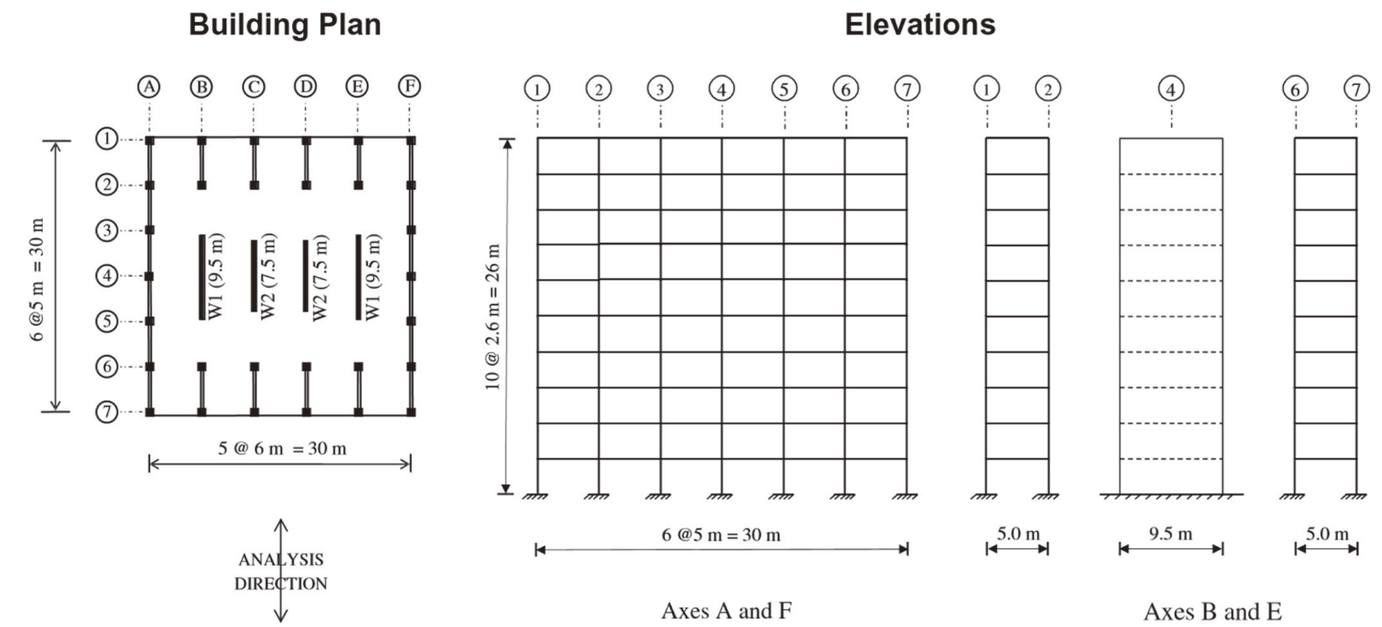

Fig. 6. Description of the 10-story RC dual wall-frame building [16].

Table 1
Natural periods of the studied buildings.

Structural system	Floors	Nomenclature	Fundamental period T_1 (s)	Second natural period (s)	Third natural period (s)
Steel frames	3	3S	0.97	0.33	0.18
	9	9S	2.10	0.80	0.47
	20	20S	3.56	1.23	0.71
Reinforced concrete walls	5	5RCW	0.24	0.06	0.03
	10	10RCW	0.62	0.15	0.07
	20	20RCW	1.09	0.30	0.14
Reinforced concrete walls and frames	10	10RCWF	0.71	0.18	0.08

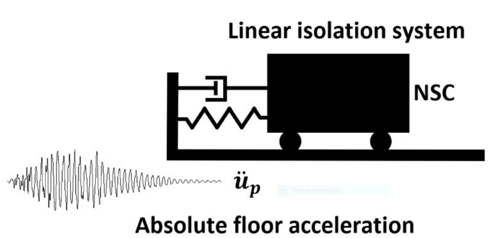

Fig. 7. Linear isolation system for NSCs.

buildings considered are exposed to this type of seismic excitations [35]. Since floor accelerations are mainly influenced by the dynamic characteristics of buildings [37], the results are expected to be similar when considering near-field pulse motions or accelerations on soft soils. However, this assumption must be verified using such types of seismic excitations.

A total of seven buildings were subjected to the thousand simulated seismic excitations and the corresponding absolute floor accelerations were obtained for each building. Three of these buildings are steel buildings with 3, 9 and 20 floors and were developed by the SAC Phase II Steel Project considering the seismic hazard corresponding to Los Angeles, USA [40]. A schematic description of the 3-story steel building is shown in Fig. 4. The 9-story and 20-story steel buildings have similar characteristics; detailed information on them can be found in the study by Ohtori et al. [40].

In addition, three reinforced concrete wall buildings of 5, 10 and 20 stories were also considered. The characteristics of these buildings are typical of traditional reinforced concrete wall buildings built in Chile [49]. Although these last three buildings are not real buildings, they are a good representation of the general behavior of this structural system. Fig. 5 shows the 5-story RC wall building; the other RC wall buildings have similar characteristics, complete details of the RC wall buildings are in the study of [49]. Finally, a 10-story reinforced concrete wall and frame dual system building was also considered for the analysis. The characteristics of this building are representative of more recent buildings built in Chile [16]. The characteristics of this building are shown in Fig. 6, full details of this building can be found in the study of [16]. Table 1 lists the natural periods of the buildings considered and the nomenclature used to refer to them.

The absolute acceleration response of the building models for each floor level was obtained by time history analysis. Then, the response of a given NSC for each floor acceleration history of a building was obtained independently of the building, therefore the interaction between the NSC and the building was not considered, this analysis is often referred to as "cascade analysis" and is accurate when the mass of the NSC is much smaller than the mass of the building, which is true for the vast majority of cases. In this setting, the maximum acceleration response of rigid NSCs is obtained directly from the analysis of the buildings and is equal to the PFA of the floor to which the NSC is anchored. The acceleration demand of the NSC was then determined as the median of the responses, i.e., the median of the thousand absolute accelerations. All building models were assumed to have linear elastic behavior, and all results were obtained by time-history analysis. The applicability of the results obtained for elastic buildings to inelastic buildings is evaluated by considering three RCFBs.

Table 2
Parameters used for the linear isolation systems.

Building	Linear isolation system	
	Criticial damping ratio	Isolation period (s)
3S	0–0.5	0–6
9S	0–0.5	0–8
20S	0–0.5	0–9
5RCW, 10RCW, 10RCWF and 20RCW	0–0.5	0–6

3. Linear isolation system and global isolation period

Once the absolute accelerations at each floor of the buildings were obtained, the seismic response of the NSC equipped with a linear seismic isolation system was numerically modeled. This system is represented by a spring and a viscous damper arranged in parallel, and it is characterized by two fundamental parameters: the isolation period T_b and the damping ratio ξ_b. In practice, this system can be implemented through a support device consisting of a spring and a viscous damper, to which the rigid NSC is attached (Fig. 7). The equation of motion describing this system corresponds to that of a single-degree-of-freedom oscillator and, therefore, is expressed by Eq. (7) [7].

$$m\ddot{u} + c\dot{u} + ku = -m * \ddot{u}_p \tag{7}$$

where $\ddot{u}$, $\dot{u}$ and u represent, respectively, the acceleration, velocity, and displacement of the NSC with respect to the equilibrium position of the linear isolator, while $\ddot{u}_p$ denotes the absolute acceleration of the floor to which the NSC is anchored. In this study, a wide range of damping ratios and isolation periods of the system were considered, as summarized in Table 2.

Fig. 8a presents the results of the absolute acceleration of a rigid NSC equipped with a linear isolation system and subjected to ground accelerations. The results are shown for different combinations of isolation periods on the Y-axis and damping ratios of the isolation system on the X-axis. These values are normalized with respect to the maximum response of the NSC without isolation; since the NSC is rigid, the

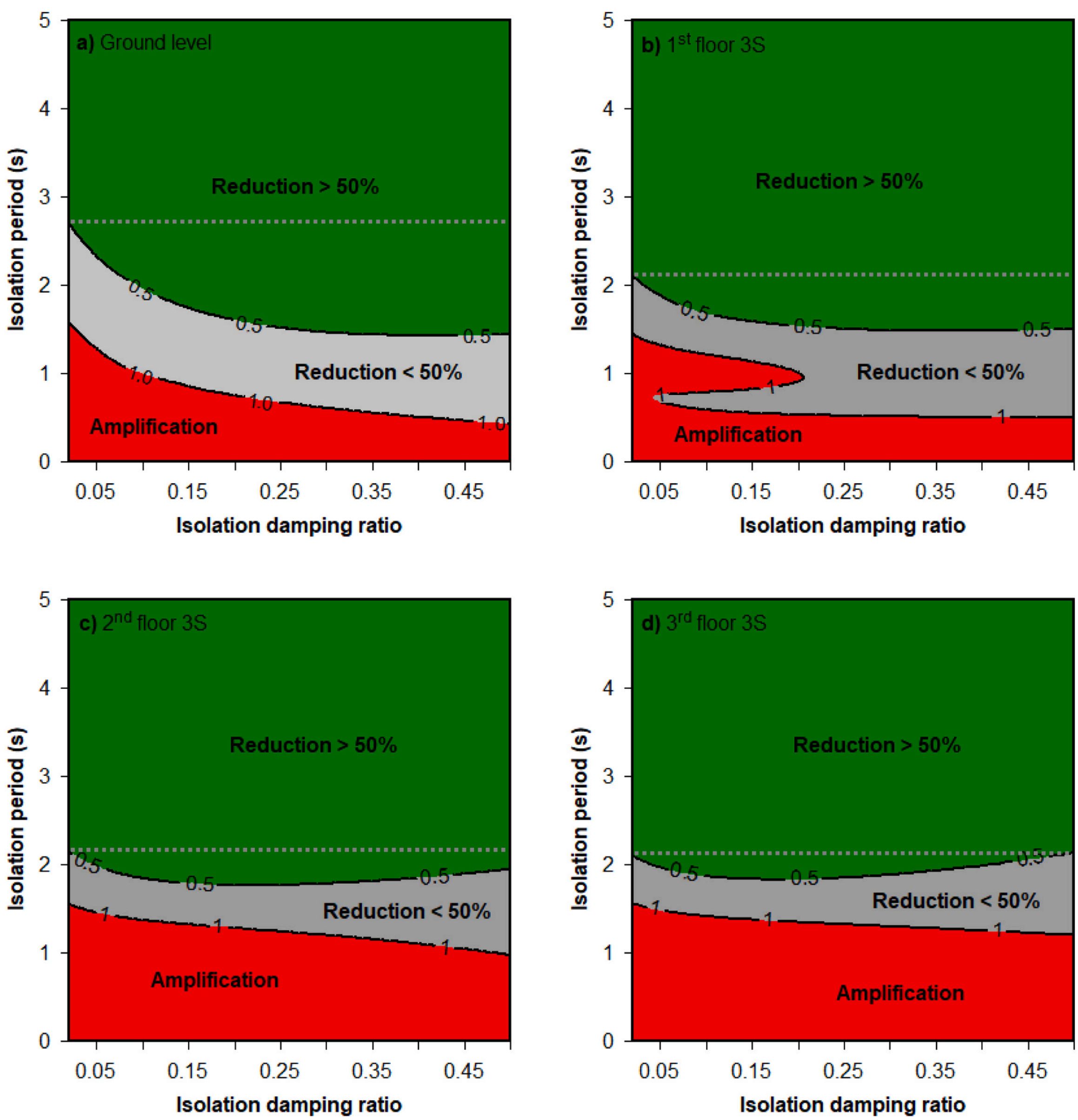

Fig. 8. Normalized acceleration demands with respect to PGA and PFA in rigid NSCs equipped with linear isolation. Results for NSCs located at ground level and on the first, second, and third floors of the three-story steel structure (3S).

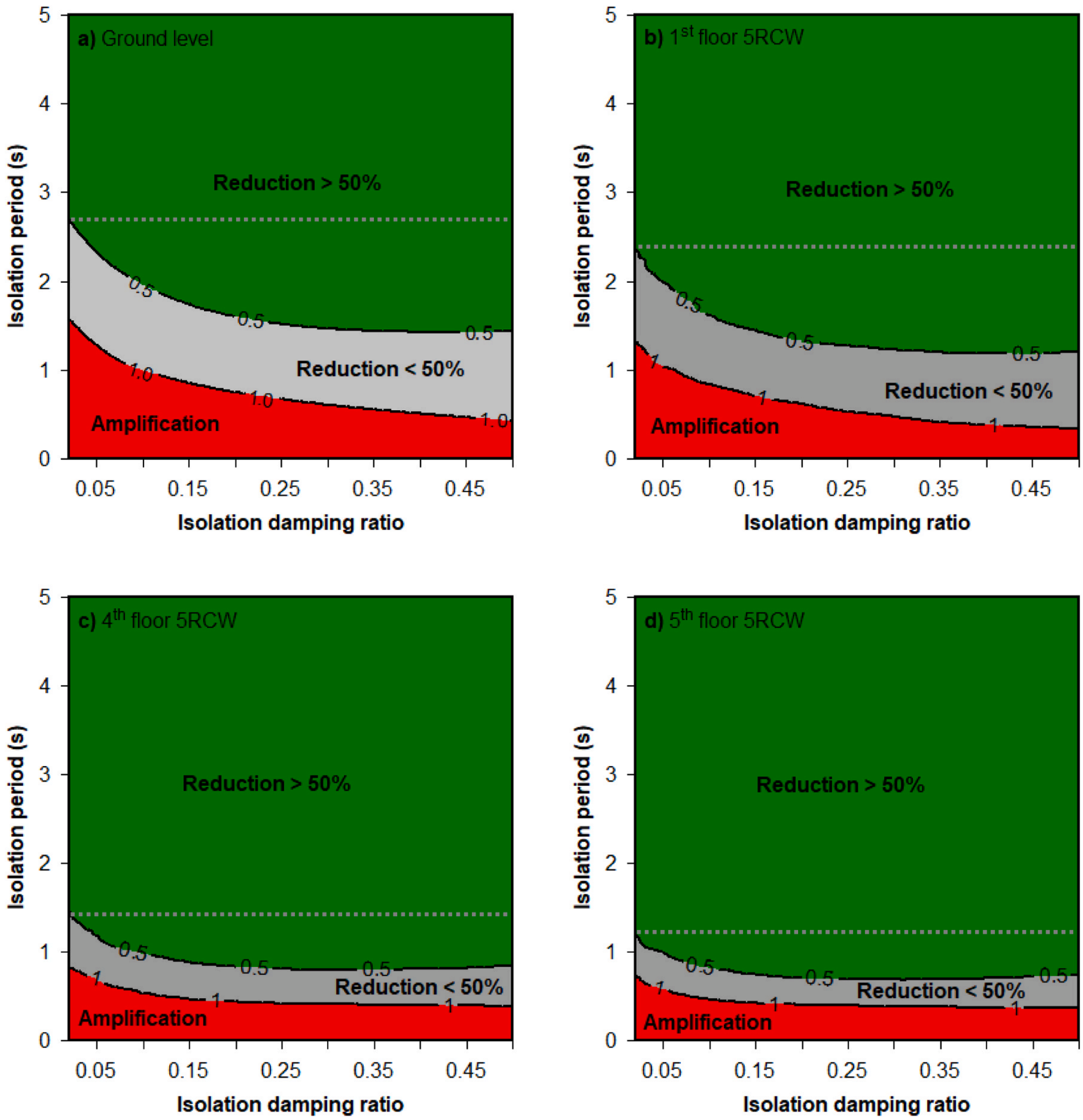

Fig. 9. Normalized acceleration demands with respect to the FPA in rigid NSCs with linear isolation, located on different floors of the 5-story RC wall structure (5RCW).

Table 3
Values of T_g/T_1 of the buildings considering different levels of reduction in the acceleration demand of the NSC.

Structure	Fundamental period T_1(s)	T_g/T_1 depending of percentage reduction					Determinant floors of T_g
		50%	60%	70%	80%	90%	
5RCW	0.24	10.0	10.8	13.5	16.3	21.7	1
10RCW	0.62	4.0	4.5	5.5	6.5	8.9	1
10RCWF	0.71	3.5	3.9	4.8	5.6	7.7	1
3S	0.97	2.3	2.4	2.8	3.3	4.5	1, 2 and 3
20RCW	1.09	2.3	2.6	2.9	3.5	4.8	1–4 and 12–17
9S	2.10	1.8	1.9	2.1	2.4	1.8	7 and 8
20S	3.56	1.4	1.5	1.6	1.8	2.3	16–18

normalization is performed with respect to the Peak Ground Acceleration (PGA). The results are grouped into three zones, identified by different colors, which represent varying levels of isolation system efficiency. The green zone corresponds to values lower than 0.50 and represents isolation system configurations that achieve reductions in the NSC response greater than 50%. This region is labeled as "Reduction > 50%" and is bounded by the curve associated with the value of 0.5. On this curve lie all combinations of isolation period and damping ratio that produce an exact 50% reduction in the maximum acceleration of the NSC.

The second zone, shown in gray, corresponds to values between 0.50 and 1.00. This region includes the isolation system configurations that

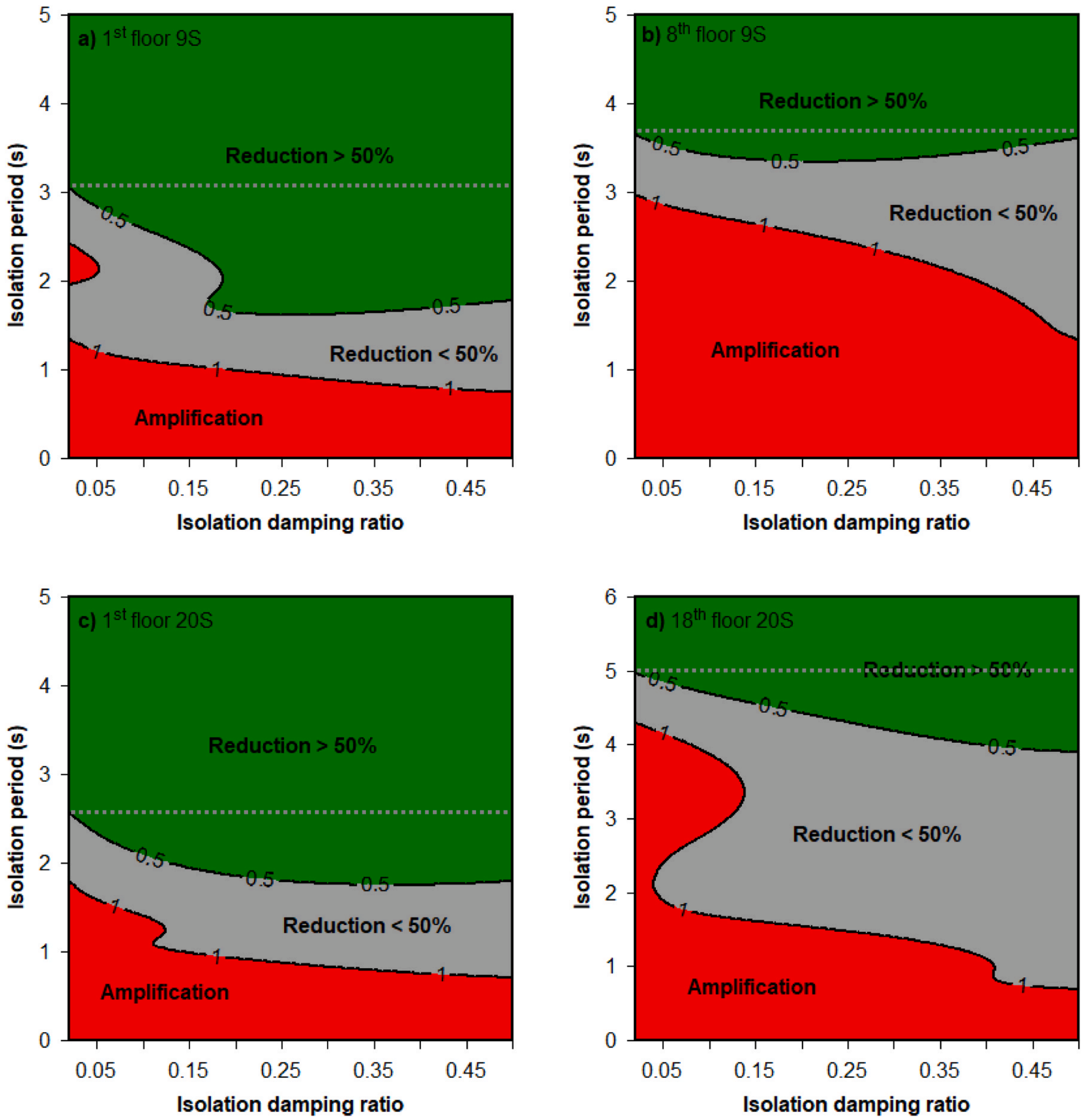

Fig. 10. Normalized acceleration demands with respect to the PFA in rigid NSCs with linear isolation: a) first floor, 9S; b) eighth floor, 9S; c) first floor, 20S; d) 18th floor, 20S.

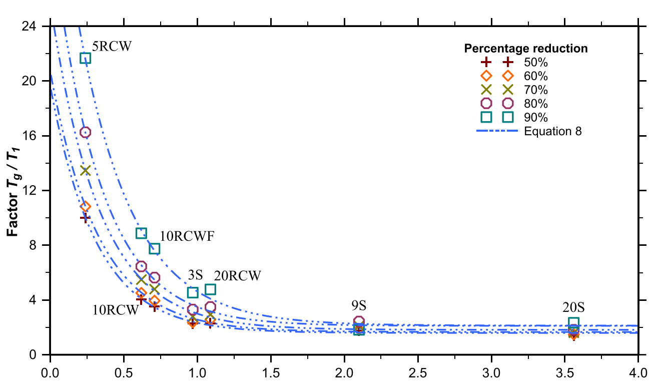

Fig. 11. Normalized results of the global isolation period T_g/T_1, as a function of the fundamental period T_1, for the seven buildings studied. Comparison of results with Eq. (8).

Table 4
Values of the coefficients of Eq. (8) as a function of the percentage reduction in the acceleration demand in the NSCs.

–	Reduction percentaje				
	50%	60%	70%	80%	90%
	(r = 0.9990)	(r = 0.9985)	(r = 0.9986)	(r = 0.9986)	(r = 0.9984)
A	1.59	1.66	1.82	2.11	2.13
B	18.10	19.05	23.97	29.36	37.23
C	-3.19	-3.05	-3.01	-3.05	-2.70

produce reductions in the NSC response of less than 50% and is labeled as “Reduction < 50%”. Its limits are defined by the curves associated with the values of 0.5 and 1.0. The third zone, shown in red, corresponds to values greater than 1.0 and represents the combinations of isolation period and damping ratio that lead to an amplification of the NSC response. This region is labeled as “Amplification” and is bounded by the curve with the value of 1.0. In addition, Fig. 8a shows a gray dashed

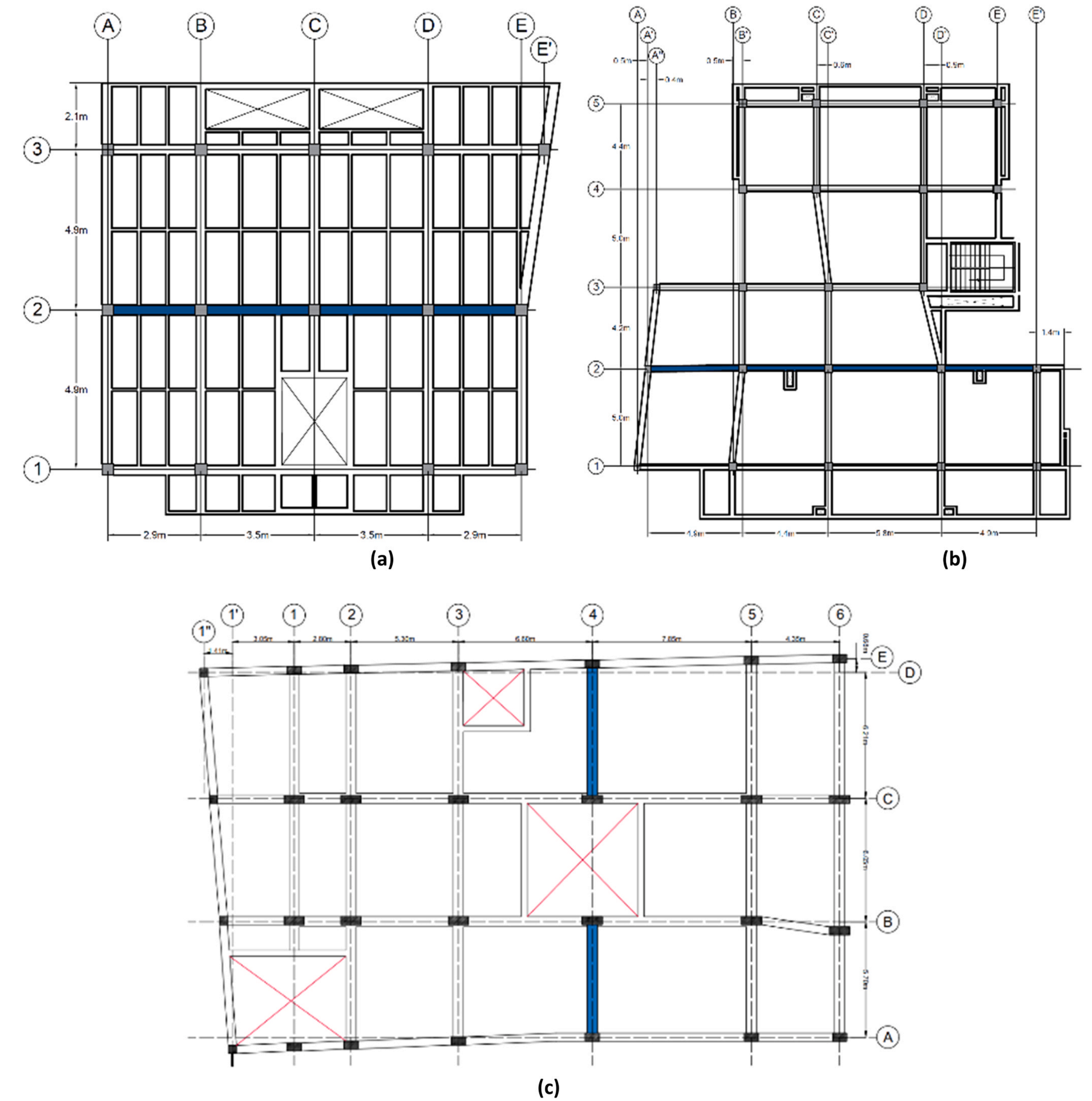

Fig. 12. Plan layout of the buildings: (a) 3 F, (b) 4 F, (c) 14 F.

horizontal line indicating that isolation periods longer than approximately 2.6 s ensure reductions in the NSC response greater than or equal to 50%, regardless of the damping ratio adopted for the isolation system.

Figs. 8b, 8c, and 8d present results similar to those shown in Fig. 8a, with the difference that the input considered to determine the response of the NSC with the isolation system corresponds to the floor accelerations of the 3-story steel building. The results were normalized with respect to the maximum acceleration of the NSC without isolation; that is, in each case, the normalization was carried out with respect to the PFA of the corresponding floor. Each figure also shows a gray dashed horizontal line indicating the minimum isolation period required to ensure reductions greater than 50%, regardless of the damping ratio of the isolation system. It can be observed that, for all three floors of the building, this period is approximately 2.2 s. In other words, as long as the isolation period of the NSC is equal to or greater than 2.2 s, its response will fall within the green zone of Figs. 8b, 8c, and 8d, irrespective of the damping ratio adopted.

By considering the gray dashed lines in the four graphs of Fig. 8, it can be observed that an isolation period of 2.6 s for the NSC guarantees reductions equal to or greater than 50%, regardless of the damping ratio adopted in the isolation system and the position of the NSC within the building, including the ground level. This value is referred to as the *global isolation period* of the NSC for the 3-story steel building, defined as the minimum isolation period that ensures the target maximum acceleration response of the NSC, independent of its location within the building and of the damping ratio of the isolation system. For simplicity,

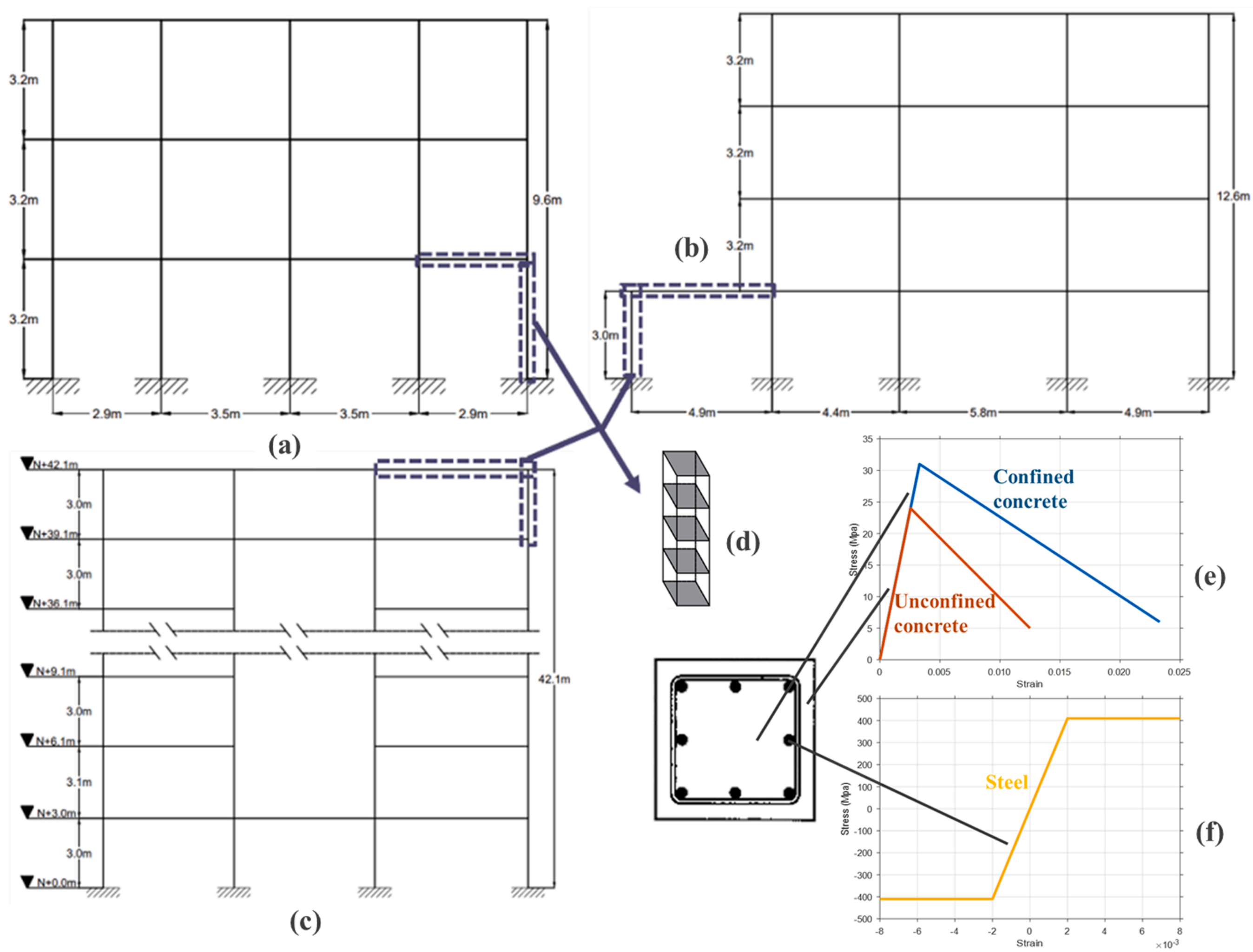

Fig. 13. Numerical models of the 3 F, 4 F and 14 F buildings. (a) Elevation view of the 3 F building, (b) Elevation view of the 4 F building, (c) Elevation view of the 14 F building, (d) Fiber sections beams and columns, (e) Backbone curve of unconfined and confined concrete of the columns, and (f) Backbone curve of the rebar.

this period is denoted as T_g. The determination of T_g is important, as it simplifies the design of isolation devices for rigid NSCs. It is important to clarify that the reduction in the acceleration demand of the NSC varies with the damping ratio of the isolation system and the position of the NSC within the building. However, the purpose of T_g is to ensure a reduction of at least 50%, regardless of the damping selected for the isolation system or the location of the NSC in the building.

Fig. 9 presents results similar to those shown in Fig. 8, but in this case considering the accelerations at the ground level and at floors 1, 4, and 5 of the 5-story reinforced concrete building (5RCW). As in the 3-story steel building, the four figures include a gray dashed horizontal line that represents the minimum isolation period required to achieve a reduction in the NSC response greater than or equal to 50%, regardless of the damping ratio adopted for the isolation system. The largest of these periods corresponds to the T_g of the building, which is governed by the ground accelerations (Fig. 9a) and has a value of 2.6 s.

Since the building is rigid, the results at the first floor (Fig. 9b) are similar to those obtained at the ground level, requiring a comparable isolation period. However, when considering the accelerations at the upper floors, the required isolation periods decrease, from 2.4 s at the first floor to 1.2 s at the roof level. This behavior occurs because, at the upper stories, the accelerations are more strongly influenced by the building's natural periods, which for the 5RCW are relatively low ($T_1 = 0.26$ s and $T_2 = 0.06$ s). Furthermore, it has been observed that damping becomes less effective in reducing the NSC response as it is placed at higher floors of the building.

In the 10-story reinforced concrete building (10RCW), a behavior analogous to that of the 5-story building is observed; for simplicity, these results are not included. Since the structural system of the building is rigid and the first two floors are close to the ground level, the results for these floors are similar to those obtained for ground accelerations. In contrast, at the upper levels, the results differ due to the greater influence of the natural periods of the building on the frequency content of the floor accelerations ($T_1 = 0.62$ s, $T_2 = 0.15$ s). The minimum isolation period required to achieve reductions greater than 50% varies from 2.4 s at the second floor to 1.5 s at the upper floors. As in the case of the 5-story building, the period T_g is governed by the ground accelerations and is equal to 2.6 s.

In the 20-story reinforced concrete building (20RCW), whose fundamental period is longer than that of the 5RCW and 10RCW buildings, the upper-intermediate levels (floors 12–17) require isolation periods close to 2.5 s, similar to those obtained at ground level. Likewise, the first four floors exhibit greater stiffness compared to the lower floors of the 5RCW and 10RCW buildings; consequently, the results for floors 1–4 are analogous to those at the ground. Thus, the global period for this building remains 2.6 s, with the difference that it is governed by the accelerations of multiple levels, specifically floors 1–4 and 12–17 (Table 3).

Fig. 10 presents the results associated with the 9- and 20-story steel buildings (9S and 20S). The results of these steel buildings differ from

Table 5
Dimensions of cross-sections for 3, 4 and 14-story buildings.

Building	Section ID	Cross-section characteristics	
		Section dimensions (m)	Longitudinal rebars
3 F (T_1 = 0.54 s)	3C1	0.35 × 0.35	8#6
	3C2	0.35 × 0.35	12#5
	3 V	0.30 × 0.35	2#6 + 3#4 (Top), 4#4 (Bottom)
4 F (T_1 = 0.67 s)	4C1	0.30 × 0.30	8#5
	4C2	0.40 × 0.40	12#5
	4V1	0.30 × 0.35	4#5 (Top), 2#5 (Bottom)
	4V2	0.30 × 0.35	2#6 + 2#5 (Top), 2#5 (Bottom)
	4V3	0.30 × 0.35	2#6 + 2#5 (Top), 3#5 (Bottom)
	4V4	0.30 × 0.35	2#7 + 2#5 (Top), 3#5 (Bottom)
14 F (T_1 = 1.14 s)	14C1	0.40 × 0.70	20#7
	14C2	0.40 × 1.00	28#8
	14C3	0.40 × 0.80	24#8
	14C4	0.40 × 0.70	20#8
	14V1	0.60 × 0.50	4#6 + 2#5 (Top), 5#6 (Bottom)
	14V2	0.95 × 0.50	2#6 + 4#5 (Top), 2#6 + 4#5 (Bottom)
	14V3	0.80 × 0.50	9#7 (Top), 5#7 + 2#6 (Bottom)
	14V4	0.50 × 0.50	6#7 + 2#5 (Top), 4#6 (Bottom)

those of the reinforced concrete buildings, since in the case of steel buildings the frequency content of the floor accelerations is more strongly dominated by the natural periods, even at the lower levels (Figs. 8b and 10a). For example, in the 3-story steel building (3S), the global isolation period is 2.2 s; this minimum period required to achieve reductions greater than 50% is similar across all floors and smaller than that associated with ground accelerations (2.6 s). The same trend is observed in the 9-story steel building (9S), where the fundamental period ($T_1 = 2.1$ s) significantly influences the accelerations of all floors. In this building, unlike what was observed in reinforced concrete buildings, damping plays a relevant role in reducing the response, and the global period T_g reaches a value of 3.7 s, governed by the upper floors (7 and 8), as shown in Fig. 10b.

In the 20-story steel building, the first two floors exhibit similarities with the ground accelerations, requiring a minimum period of 2.6 s. However, from the third floor upward, the influence of the natural periods becomes dominant. Since this building has the largest fundamental period, the global period required to achieve significant response reductions reaches 5.0 s and is governed by the upper floors (16−18). In this case, the isolation system presents an important limitation due to the need for such a long period. For these cases, a specific analysis of the floor where the NSC will be anchored must be carried out. As shown in Fig. 10d, one alternative is to provide high damping to the isolation system, close to 40%, which allows reducing the required isolation period to achieve a target reduction. The values of the global isolation period and the controlling levels for all buildings are presented in Table 3.

The analysis initially considered, in an arbitrary manner, a reduction in the accelerations of NSCs equal to or greater than 50% compared to the response without the isolation system. When repeating the analysis for higher reduction thresholds, the values indicated in Table 3 were obtained, expressed in terms of the T_g/T_1 ratio. These results are valid for damping ratios between 0% and 50%.

The results in Table 3 are organized as a function of the fundamental period of the buildings and show a clear relationship between this parameter and the T_g/T_1 ratio. Fig. 11 presents the variation of this ratio as a function of T_1 and the percentage reduction in the NSC accelerations. The results indicate that the T_g/T_1 ratio decreases exponentially with increasing T_1, stabilizing at values close to 2. This trend is considered generalizable to regular buildings with different fundamental periods.

Given the clear trend observed in the curves of Fig. 11, a regression analysis was performed, leading to Eq. (8)

$$\frac{T_g}{T_1} = A + Be^{CT_1} \tag{8}$$

where the constants A, B, and C depend on the percentage of response reduction and are presented in Table 4. Fig. 11 shows the agreement between the simulated values and those estimated using Eq. (8), which demonstrates the usefulness of the latter for estimating the global isolation period of a system applied to NSCs, as a function of the building's fundamental period and the required level of acceleration reduction.

4. Validation of the global isolation period

Since Eq. (8) uses linear models for buildings and the NSC isolation system and since buildings and seismic isolation devices usually operate within the inelastic range, this section employs numerical simulations to assess the equation's accuracy. Three inelastic models of three RCFBs representative of this structural system are used. Additionally, an inelastic seismic isolation system (frictional pendulum system, FPS) is considered for the NSCs.

4.1. Buildings and seismic excitations used for the validation of the global isolation period

Three RCFBs located in Colombia with 3, 4, and 14 floors were selected for the validation of the global isolation period equation (Eq. (8)). Fig. 12 shows the plan layout of the selected buildings, hereafter referred to as 3 F, 4 F, and 14 F, with blue frames indicating those selected for OpenSeesPy 2D modelling. The numerical models of the three buildings are shown in Fig. 13. The dimensions of the building sections are listed in Table 5 and shown in Figs. 14a, 14b and 14c. Fig. 14d shows the fiber element integration points for the 3 F building.

The dead loads (DL) for all three buildings were 3 kN/m^2, while the live loads (LL) for floors and roofs were set at 1.8 kN/m^2 and 0.5 kN/m^2, respectively. The buildings were designed in accordance with the Colombian Code for earthquake-resistant construction (AIS-2017). This code is similar to the ACI 318–08 in their requirements for reinforced concrete frames buildings. Design spectral accelerations were determined using seismic risk zones and soil types prescribed in the AIS-2017 code. For instance, building 3 F in Cartagena, Colombia, with a fundamental period of 0.54 s, has a design spectral acceleration of 0.40 g (without dividing by the R factor), while building 14 F in Barrancabermeja, Colombia, with a fundamental period of 1.14 s, has a design spectral acceleration of 0.33 g. Concrete compressive strength (f'_c) varies between buildings, with values of 21 MPa, 24.5 MPa, and 28 MPa for buildings 3 F, 4 F, and 14 F, respectively. Young's modulus of steel (E_s) is set to 210 GPa.

In Colombia, most commercial reinforcing bars have a yield strength of 420 MPa, so this constant value (f_y) was used in the reinforcement modelling. Distributed plasticity models for reinforced concrete were used to represent the inelastic behavior along the sections of the members. The Mander model [31] was used to simulate the confined concrete, considering maximum compressive strengths of 27.3 MPa, 31.9 MPa and 36.4 MPa in the 3 F, 4 F and 14 F buildings, respectively. The modelling approach included fixed base conditions and mass assignment at the model nodes. The seismic mass at each node was determined by distributing the basal shear of the column to the nodes according to Eq. (9).

$$\text{NodeMass} = \frac{V_b}{S_{ad} g N_f} \tag{9}$$

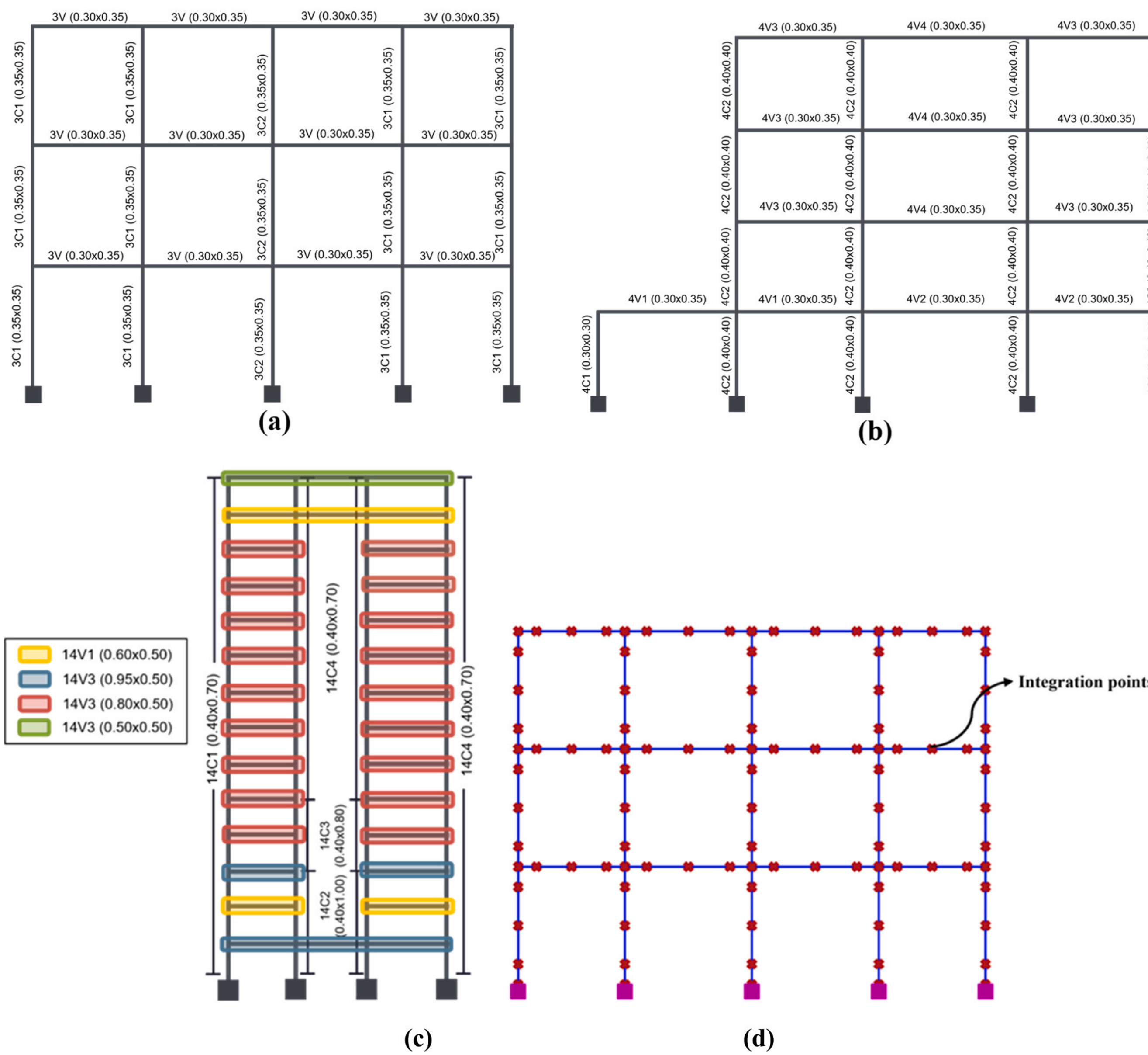

Fig. 14. Beam and column cross-sections of the buildings: (a) 3 F, (b) 4 F, (c) 14 F, (d) Integration points of the fiber elements for the 3 F building.

where Sa_d is the corresponding value of the design spectrum (expressed in units of g), g is the acceleration of gravity in m/s^2 and N_f is the number of floors of the building used to distribute the shear between the nodes. The mass assigned to each node is called NodeMass, while V_b is the basal shear of the column between the nodes. The structural elements were modelled using the forceBeamColumn formulation in OpenSeesPy, with five integration points per element according to a Gauss-Lobatto scheme. Linear transformations were applied to the beams and P-Delta transformations to the columns. To ensure uniform horizontal displacements at the nodes on the same floor, a rigid diaphragm was imposed on each floor by a constraint with equal degrees of freedom.

Both confined and unconfined concrete were modelled using the Kent-Scott-Park model without tensile capacity, implemented using the Concrete01 material in OpenSeesPy. The residual strength of the concrete was assumed to be 20% of its ultimate compressive strength (f'_c). The strain corresponding to the maximum compressive strength for both types of concrete was determined using the expression $\varepsilon_c = \frac{2f'_c}{E_c}$, where E_c is the modulus of elasticity of the concrete.

The applied load combination for permanent loading was 1.05DL + 0.25LL. The rebar was simulated using the Steel01 material model in OpenSeesPy. To improve the model, steel rupture and buckling effects were incorporated through the MinMax material, which defines upper and lower bounds for the material response. The lower limit (-0.008) was set to represent bar buckling after concrete spalling, while the upper limit (0.05) accounted for low cycle fatigue effects.

Since the buildings are in Colombia and the seismic hazard in this region is influenced by different types of seismic genesis, it was decided to select the set of seismic records proposed in FEMA document P-695 [12]. Fig. 15a shows the individual response spectra and the average response spectrum of these records. First, each seismic record was scaled so that the spectral ordinate at the fundamental period of the building matched the design spectral ordinate, whose values were 0.40 g, 0.37 g and 0.33 g for the 3 F, 4 F and 14 F buildings, respectively. The scaled response spectra of each seismic data set, together with the average spectrum of the seismic records, are shown in Figs. 15b, 15c and 15d for the 3 F, 4 F and 14 F buildings, respectively.

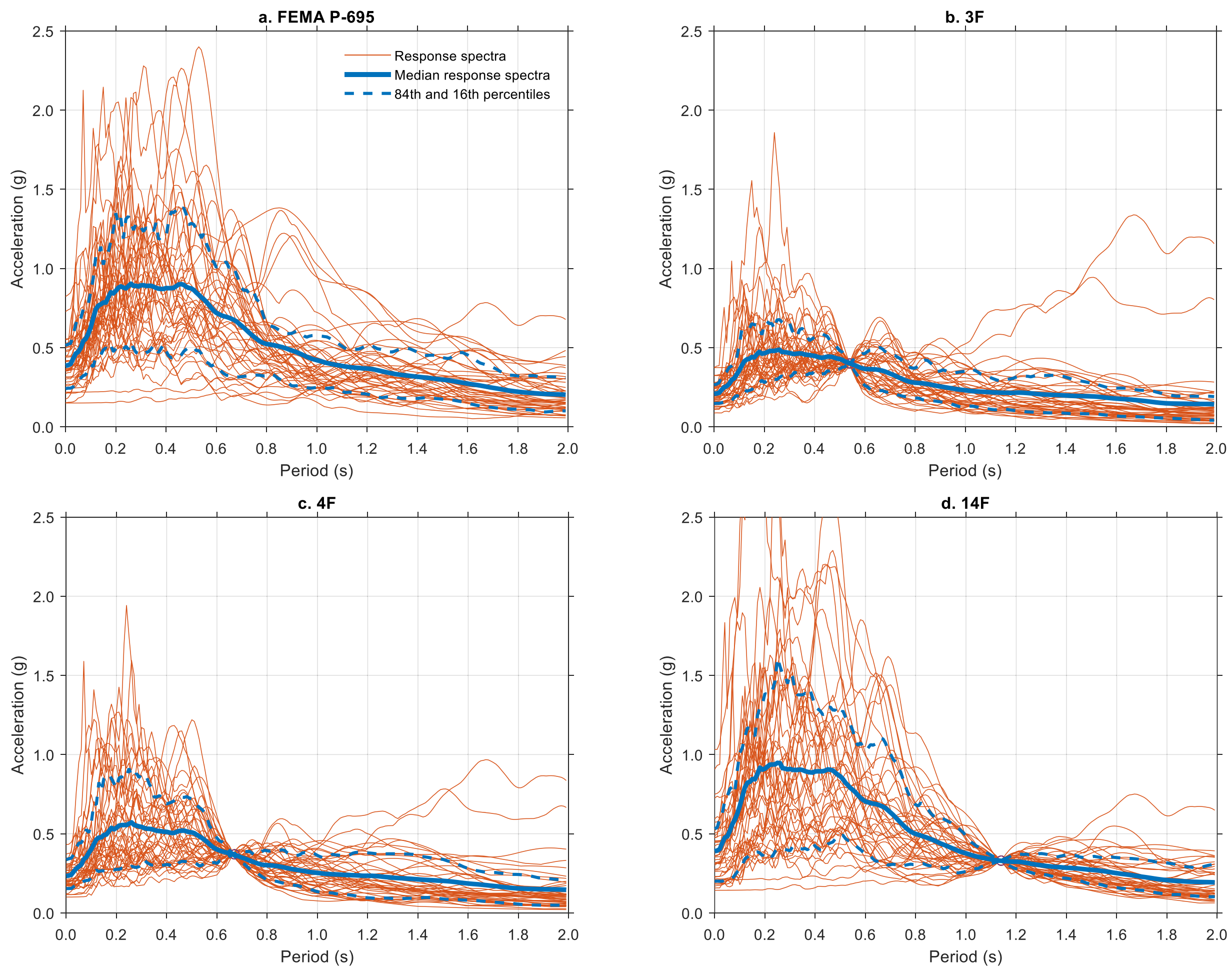

Fig. 15. Acceleration response spectra: a) FEMA P-695 records, b) scaled records for structure 3 F, c) scaled records for structure 4 F and d) scaled records for structure 14 F.

4.2. Isolation system used for the validation of the global isolation period

The global isolation period of the NSCs was validated using the Frictional Pendulum System (FPS). The FPS is modeled as a system that generates a bilinear force-deformation relationship, and it is characterized by two parameters: the radius of curvature R of the sliding surface and the coefficient of friction μ. The equation of motion of the FPS [8] can be obtained from Fig. 16. When the force equilibrium is performed in the horizontal x-direction, the following is obtained:

$$F_x = ma_x \tag{10}$$

$$-\mu N\cos\theta - N\sin\theta = m * (\ddot{u}_p + \ddot{u}_x) \tag{11}$$

where $\ddot{u}_p$ is the absolute acceleration of the floor on which the NSC will be anchored, $\ddot{u}_x$ is the acceleration of the NSC with respect to the equilibrium point of the FPS, μ is the friction coefficient of the FPS, N is the force normal to the friction surface, m is the mass of the rigid NSC, and θ is the angle formed by the current position of the NSC with respect to its equilibrium position. On the other hand, if the forces in the vertical direction Y are considered, the following equation of motion is obtained:

$$F_y = ma_y \tag{12}$$

$$N\cos\theta - mg - \mu N\sin\theta = m\ddot{u}_y \tag{13}$$

if it is considered that the angle θ is small and also that the friction coefficient μ is much less than 1, then $\ddot{u}_y \approx 0$ and $\mu.sin(\theta) \approx 0$. Taking these considerations into account, the above equation can be written as follows:

$$N\cos\theta - mg = 0 \tag{14}$$

solving for N yields the following:

$$N = \frac{mg}{\cos\theta} \tag{15}$$

by replacing Eq. (15) in Eq. (11), we obtain the following:

$$-\mu\frac{mg}{\cos\theta}\cos\theta - \frac{mg}{\cos\theta}\sin\theta = m * (\ddot{u}_p + \ddot{u}_x) \tag{16}$$

if we now consider that $\sin\theta = u_x/R$ and that, for small angles, (less than 25°) $\cos\theta \approx 1$, we obtain the following:

$$-\mu mg - mg\frac{u_x}{R} = m * (\ddot{u}_p + \ddot{u}_x) \tag{17}$$

if we also consider that the weight of the NSC is equal to $W = mg$, the equation takes the following form:

$$m * (\ddot{u}_p + \ddot{u}_x) = -W\mu - W\frac{u_x}{R} \tag{18}$$

which gives the force versus displacement ratio of the FPS is obtained:

$$F = -W\mu - W\frac{u_x}{R} \tag{19}$$

Eq. (19) can be further simplified by dividing by the mass m of the NSC, which makes the equation of motion becomes mass independent

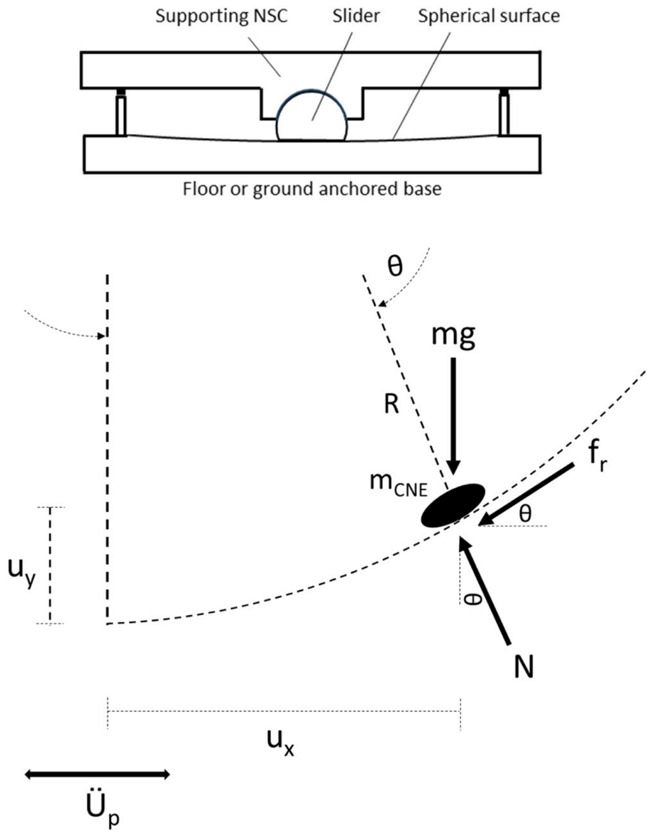

Fig. 16. Diagram of the acting forces in the NSC with a Frictional Pendulum System (FPS).

and takes the following form:

$$\ddot{u}_p + \ddot{u}_x = -\mu g - g\frac{u_x}{R} \tag{20}$$

the previous equation has a component relative to the frictional force of the FPS equal to $-\mu g$, the direction of this force is variable and depends on the sign of the NSC velocity, for this reason it is convenient to add the sign function called *sign* for the correct assignment of this force. With this consideration the equation of motion finally takes the form of Eq. (21):

$$\ddot{u}_p + \ddot{u}_x = -\mu g sign(\dot{u}_x) - g\frac{u_x}{R} \tag{21}$$

The solution of this nonlinear ordinary differential equation was performed by numerical integration using the Runge-Kutta 4–5 numerical integrator through MatLab software.

It is important to note that when the friction coefficient and the horizontal displacements are small (less than *0.4 R*), the dynamic behavior of the FPS is similar to that of a simple pendulum with small amplitude, and an approximate period of oscillation or isolation can be associated with Equation (22) [29]:

$$2\pi(R/g)^{1/2} \tag{22}$$

The above equation can be used to estimate the radius of curvature of the FPS associated with the design isolation period of the FPS.

4.3. Results of validating the global isolation period

Fig. 17 shows the median Peak Floor Accelerations (PFAs) of the buildings, Fig. 17a shows the results of the PFAs in *g* units and Fig. 17b shows the results of the PFAs normalized with respect to the Peak Ground Accelerations (PGAs). Except for the 14 F building, and consistent with the results of previous studies [14,37,39,41,47], PFAs increase steadily as you move up in buildings. The values shown in Fig. 17 represent the peak acceleration demands of rigid NSCs without seismic isolation systems.

Fig. 18 shows the reduction in absolute accelerations of the rigid NSCs obtained when provided with the FPS and when subjected to the different accelerations of the buildings. Equation (22) was used to determine the radius of curvature of the FPS and Eq. (8) was used to determine the design isolation period of the FPS (global isolation period). Two scenarios were considered for the use of Eq. (8): the first scenario considers a target reduction of the accelerations in the NSCs of 50% (Figs. 18a, 18c and 18e) and the second scenario considers a target reduction of 70% (Figs. 18b, 18d and 18f). The coefficients used in Eq. (8) for each case are shown in Table 4 and the results obtained for the isolation period and radius of curvature for each case are shown in Table 6. For each case, several friction coefficients corresponding to a typical range of the FPS system (between 0.03 and 0.10) were considered.

Fig. 18 shows that, for the target reduction of 50% (Figs. 18a, 18c and 18e) and for any floor of the three buildings (solid lines), and furthermore, for any value of the friction coefficient μ, Eq. (8) provides a global isolation period for the FPS that generates reductions in the

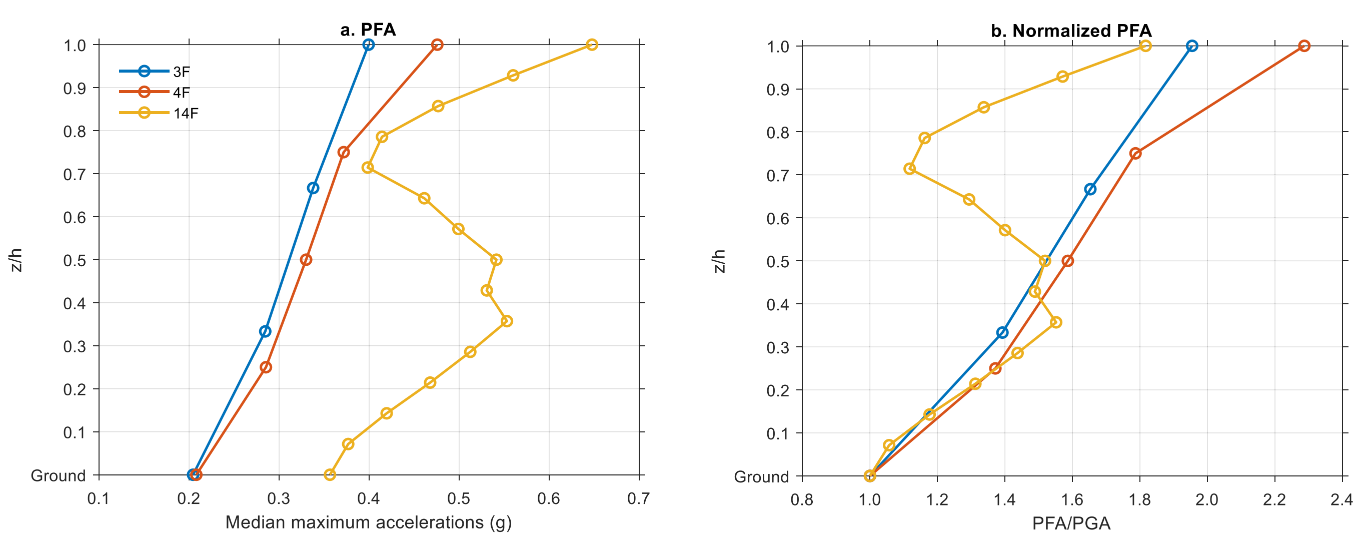

Fig. 17. Median maximum absolute accelerations of the three buildings: a) values in units of g and b) values normalized by the PGA (Peak Ground Acceleration).

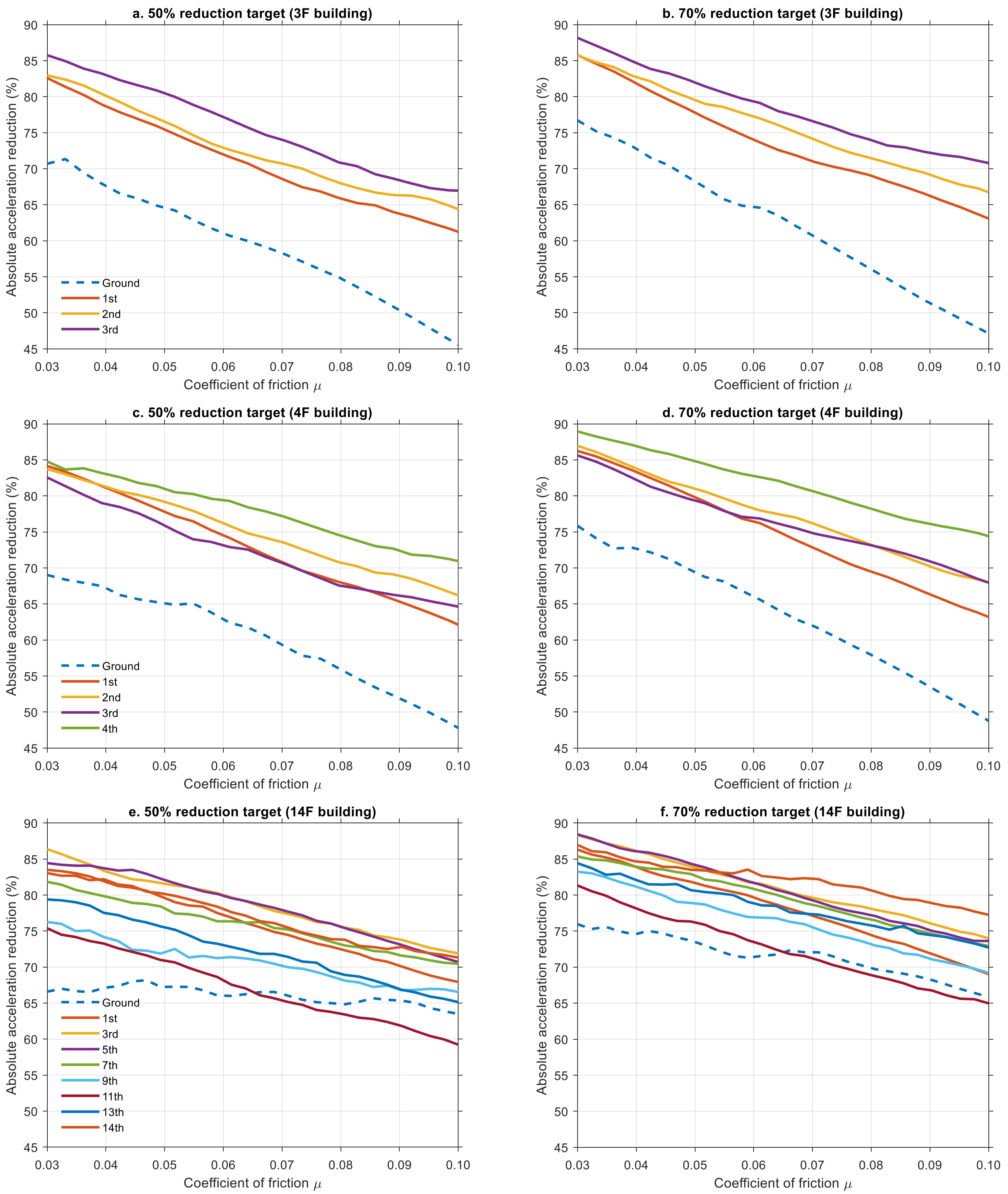

Fig. 18. Absolute acceleration results of the NSCs provided with FPS designed with the approximate global isolation period for a 50% and 70% response reduction and determined throughout Eq. (8).

absolute acceleration response of the NSC of more than 60%. This demonstrates that the estimation of the global isolation period using Eq. (8) is efficient for the floor accelerations of the three RCFBs.

In addition, when considering the accelerations at the ground level of buildings 3 F and 4 F (dashed blue curves in Figs. 18a, 18b, 18c and 18d), the reductions in the accelerations of the NSCs are smaller compared to the reductions obtained for the NSCs located at the floor levels of these buildings (in the same figures, solid lines). At ground

Table 6
Global isolation periods and their associated radius for the friction pendulum system.

Building	50% Reduction		70% Reduction	
	Isolation period	Radii	Isolation period	Radii
3 F	2.6	1.7	3.5	3.1
4 F	2.5	1.5	3.4	2.8
14 F	2.4	1.4	3.0	2.2

level, the reductions obtained are greater than 45%. A different behavior is observed in the results obtained with the accelerations at the base level of building 14 F (dashed blue lines in Figs. 18e and 18f), for this building the reductions in the accelerations of the NSCs considering ground accelerations are similar to those obtained considering the floor accelerations, at ground level the reduction values are higher than 62%.

As expected, for a 70% target reduction (Figs. 18b, 18d and 18f) and for all three buildings, higher reductions are achieved than for a 50% target reduction (Figs. 18a, 18c and 18e). However, considering the floor accelerations and for friction coefficients higher than about 0.08, the target reductions of at least 70% are not achieved (Figs. 18b, 18d and 18f). This is because more significant reductions in demand require longer isolation periods and generally involve larger relative displacements in the isolation system. Consequently, as the relative displacements of the FPS isolation system increase, the estimation of the device isolation period using Equation (22) loses accuracy.

In all cases the trends of the graphs are clear with an almost constant negative slope, the reductions are smaller as the coefficient of friction μ increases. In general, Eq. (8) generates a global isolation period for the FPS design that produces results close to the desired results. The estimation is especially accurate for floor accelerations while for ground accelerations the results do not fully match the target reductions.

5. Conclusions

This study analyzes the seismic response of rigid Nonstructural Components (NSCs) equipped with seismic isolation systems. First, the response of seven elastic buildings subjected to far-field ground motions is evaluated, and subsequently, the response of rigid NSCs with and without seismic isolation systems is determined. The concept of global isolation period, T_g, is introduced, and an equation for its prediction is proposed. This equation is then validated using the seismic response of rigid NSCs located in three inelastic reinforced concrete frame buildings (RCFBs) subjected to the design demand. As the seismic isolation device for the NSCs, the friction pendulum system (FPS) is employed. The main conclusions of this research are as follows:

- The global isolation period is introduced. It is defined as the minimum isolation period of rigid NSCs required to achieve a target acceleration response of the NSC, regardless of its location within the building and the damping of the isolation system.
- A prediction equation, Eq. (8), for the global isolation period has been developed that depends only on the fundamental period of the building (T_1) and the desired absolute acceleration response of the rigid NSC.
- The global isolation period prediction equation (Eq. (8)) provides reasonable values that can be used as a preliminary design tool for the NSC seismic isolation device. This is particularly relevant when the NSC is installed on multiple floors and only a single seismic isolation device is designed. Once the desired level of response reduction has been selected and the global isolation period defined, it is recommended to perform a numerical analysis to verify and, if necessary, adjust the design of the seismic isolation device.
- The global isolation period prediction equation (Eq. (8)) is less accurate when considering accelerations at the base of buildings (ground accelerations). The equation provides more conservative results when the target acceleration reduction of the rigid NSC is close to 50%, while for higher target reductions the equation provides less conservative values.
- For all the desired reductions in the absolute acceleration of the NSCs and for buildings with fundamental periods greater than 2 s, the convergence values of the T_g/T_1 factor are close to 2. However, in these cases the isolation period required for the NSC may be difficult to achieve. In such situations, it is recommended to perform a specific analysis considering the floor accelerations at the location where the NSC will be anchored.
- When rigid NSCs are located on lower floors of mid- or low-rise rigid buildings (e.g., 5 or 10-story reinforced concrete wall buildings), it is not enough to provide the NSC isolation system with a period greater than the fundamental period of the building. In addition, the isolation period must be effective in reducing the response of the NSC, considering ground accelerations.
- Although the proposed global isolation period equation provides a useful design tool for rigid NSCs, it is not applicable for flexible NSCs, also, its validation was limited to a small set of RC frames buildings and a single isolation device. Future research should extend the approach to irregular buildings and alternative isolation technologies, while also accounting for soil–structure interaction and flexible NSCs.

CRediT authorship contribution statement

Henry A. Colorado: Writing – original draft. **Diego Lopez-Garcia:** Visualization, Supervision, Methodology, Investigation, Formal analysis, Conceptualization. **Orlando Arroyo:** Writing – original draft, Validation, Investigation, Data curation. **Daniela Novoa:** Investigation, Data curation. **Juan Carlos Obando:** Writing – review & editing, Writing – original draft, Visualization, Validation, Methodology, Investigation, Formal analysis, Data curation, Conceptualization.

Funding

Financial support was provided by the Vicerectoría de Investigation at Universidad de Antioquia, Project No. 2024–72690 (Medellín, Colombia).

Declaration of Competing Interest

The authors declare that they have no known competing financial interests or personal relationships that could have appeared to influence the work reported in this paper.

References

[1] American Society of Civil Engineers. Minimum design loads and associated criteria for buildings and other structures. American Society of Civil Engineers; 2022.
[2] Anajafi H, Medina RA, Adam C. Evaluation of the floor acceleration response spectra of numerical building models based on recorded building response data. J Earthq Eng 2022;26(12):6378–402. https://doi.org/10.1080/13632469.2021.1927887.
[3] Banihashemi MirAmir, Wiebe Lydell, Filiatrault André. "Suitable engineering demand parameters for acceleration-sensitive nonstructural components". Earthq Eng & Struct Dyn 2024;53(14):4163–82. https://doi.org/10.1002/eqe.4207.
[4] Boore DM. Stochastic simulation of high-frequency ground motions based on seismological models of the radiated spectra. Bull Seismol Soc Am 1983;73(6A):1865–94. https://doi.org/10.1785/BSSA07306A1865.
[5] Cardone D, Gesualdi G. Seismic rehabilitation of existing reinforced concrete buildings with seismic isolation: a case study. Earthq Spectra 2014;30(4):1619–42. https://doi.org/10.1193/110612EQS323M.
[6] Chichino B, Peloso S, Bolognini D, Moroni C, Perrone D, Brunesi E. Towards seismic design of nonstructural elements: Italian code-compliant acceleration floor response spectra. Adv Civ Eng 2021;2021(1):4762110. https://doi.org/10.1155/2021/4762110.
[7] Chopra AK. Dynamics of Structures: Theory and Applications to Earthquake Engineering. Upper Saddle River, NJ: Prentice Hall. Inc; 1995.
[8] Christopoulos C, Filiatrault A, Bertero VV. Principles of Passive Supplemental Damping and Seismic Isolation. Iuss press; 2006.

[9] Clough RW, Penzien J. Dynamics of Structures. 2nd edition. New York, USA: McGraw-Hill; 1993.
[10] D'Angela D, Magliulo G, Cosenza E. Seismic damage assessment of unanchored nonstructural components taking into account the building response. Struct Saf 2021;93:102126.
[11] Dhakal RP, Pourali A, Tasligedik AS, Yeow T, Baird A, MacRae G, Palermo A. Seismic performance of non-structural components and contents in buildings: an overview of NZ research. Earthq Eng Eng Vib 2016;15:1–17. https://doi.org/10.1007/s11803-016-0301-9.
[12] Federal Emergency Management Agency, F.E.M.A. (2009). Quantification of building seismic performance factors FEMA P-695. Washington DC, USA.
[13] Filiatrault A, Sullivan T. Performance-based seismic design of nonstructural building components: The next frontier of earthquake engineering. Earthq Eng Eng Vib 2014;13:17–46. https://doi.org/10.1007/s11803-014-0238-9.
[14] Flores FX, Lopez-Garcia D, Charney FA. Assessment of floor accelerations in special steel moment frames. J Constr Steel Res 2015;106:154–65. https://doi.org/10.1016/j.jcsr.2014.12.006.
[15] Gavin HP, Zaicenco A. Performance and reliability of semi-active equipment isolation. J Sound Vib 2007;306(1):74–90. https://doi.org/10.1016/j.jsv.2007.05.039.
[16] Goldschmidt Pino, A.A. (2010). Aceleraciones de piso en edificios de estructuración mixta muros-marcos sometidos a excitaciones sísmicas.
[17] Ismail M, Rodellar J, Ikhouane F. An innovative isolation bearing for motion-sensitive equipment. J Sound Vib 2009;326(3):503–21. https://doi.org/10.1016/j.jsv.2009.06.022.
[18] Jain A, Surana M. In-plan distribution of peak floor acceleration demands in torsionally irregular buildings. J Build Eng 2024;90:109360.
[19] Jain A, Surana M. Peak floor acceleration demands in torsionally irregular buildings. Earthq Eng & Struct Dyn 2024;53(3):1145–67.
[20] Jia J, Gong M, Zuo Z, Wang X, Zhao Y. A novel deep learning-based method for generating floor response spectra of building structures. Eng Struct 2025;322:119058.
[21] Kazantzi AK, Vamvatsikos D, Miranda E. Evaluation of seismic acceleration demands on building nonstructural elements. J Struct Eng 2020;146(7):04020118. https://doi.org/10.1061/(ASCE)ST.1943-541X.0002676.
[22] Khechfe H, Noori M, Hou Z, Kelly JM, Ahmadi G. An experimental study on the seismic response of base-isolated secondary systems. J Press Vessel Technol 2002;124(1):81–8. https://doi.org/10.1115/1.1445795.
[23] Kumar M, Whittaker AS, Constantinou MC. Characterizing friction in sliding isolation bearings. Earthq Eng & Struct Dyn 2015;44(9):1409–25. https://doi.org/10.1002/eqe.2524.
[24] Latif I, Surana M, Banerjee A. Investigating in-structure acceleration amplification factor of RC frames using explainable artificial intelligence. Structures 2025;79:109592.
[25] Liu S, Warn GP. Seismic performance and sensitivity of floor isolation systems in steel plate shear wall structures. Eng Struct 2012;42:115–26. https://doi.org/10.1016/j.engstruct.2012.04.015.
[26] Lu LY, Lin GL. Predictive control of smart isolation system for precision equipment subjected to near-fault earthquakes. Eng Struct 2008;30(11):3045–64. https://doi.org/10.1016/j.engstruct.2008.04.016.
[27] Miranda E, Kazantzi AK, Vamvatsikos D. New approach to the design of acceleration-sensitive non-structural elements in buildings. 16th Eur Conf Earthq Eng 2018:18–21.
[28] Miranda E, Mosqueda G, Retamales R, Pekcan G. Performance of nonstructural components during the 27 February 2010 Chile earthquake. Earthq Spectra 2012;28(S1):S453–71. https://doi.org/10.1193/1.4000032.
[29] Naeim F, Kelly JM. Design of seismic isolated structures: from theory to practice. John Wiley & Sons; 1999.
[30] Novoa D, Arroyo O, Obando JC, Lopez-Garcia D, Carrillo J. Effect of Material Epistemic Uncertainty on the Seismic Response of RC Moment-Resisting Frame Buildings and Their Nonstructural Components. J Earthq Eng 2025:1–19.
[31] Mander JB, Priestley MJ, Park R. Theoretical stress-strain model for confined concrete. J Struct Eng 1988;114(8):1804–26. https://doi.org/10.1061/(ASCE)0733-9445(1988)114:8(1804).
[32] Meng W, Liu Y, Zheng W, Tan P, Li H, Zhu D, Guo F. Experimental and numerical study of a novel slope-type sliding isolation system for seismic protection of electrical equipment. Soil Dyn Earthq Eng 2026;200:109919.
[33] Mo Z, Lai B, Shu G, Chen P, Yang TY. Performance-based seismic design method of stacked modular steel building based on three-dimensional seismic isolation. Eng Struct 2025;336:120438.
[34] Mo Z, Shu G, Lai B, Ventura CE, Yang TY. Experimental behavior, numerical modeling and parameters evaluation of three-dimensional seismic isolation device. J Constr Steel Res 2024;220:108817.
[35] Obando JC, Novoa D, Arroyo O, Lopez-Garcia D, Carrillo J. Influence of the inelastic response of reinforced concrete frame buildings on the inelastic displacement and acceleration ratios of nonstructural elements. J Earthq Eng 2025. https://doi.org/10.1080/13632469.2025.2483524.
[36] Obando JC, Carrillo J, Arroyo O. Inelastic acceleration ratios for nonstructural components. Structures 2024;69:107374. https://doi.org/10.1016/j.istruc.2024.107374.
[37] Obando JC, Arroyo O, Lopez-Garcia D, Carrillo J. Seismic response of acceleration-sensitive nonstructural components in a Thin Lightly-Reinforced Concrete Wall (TLRCW) mid-rise building. Structures 2022;45:1878–901. https://doi.org/10.1016/j.istruc.2022.10.017.
[38] Obando JC, Lopez-Garcia D. Inelastic displacement ratios for nonstructural components subjected to floor accelerations. J Earthq Eng 2018;22(4):569–94. https://doi.org/10.1080/13632469.2016.1244131.
[39] Obando JC. Diseño sísmico de componentes no estructurales sensibles a la aceleración en edificios de múltiples pisos (Doctoral Thesis (in Spanish)). Santiago, Chile: Pontificia Universidad Católica de Chile; 2016.
[40] Ohtori Y, Christenson RE, Spencer Jr BF, Dyke SJ. Benchmark control problems for seismically excited nonlinear buildings. J Eng Mech 2004;130(4):366–85. https://doi.org/10.1061/(ASCE)0733-9399(2004)130:4(366).
[41] Perrone D, Calvi PM, Nascimbene R, Fischer EC, Magliulo G. Seismic performance of non-structural elements during the 2016 Central Italy earthquake. Bull Earthq Eng 2019;17:5655–77. https://doi.org/10.1007/s10518-018-0361-5.
[42] Ray-Chaudhuri S, Hutchinson TC. Effect of nonlinearity of frame buildings on peak horizontal floor acceleration. J Earthq Eng 2011;15(1):124–42. https://doi.org/10.1080/13632461003668046.
[43] Reggio A, De Angelis M. Optimal design of an equipment isolation system with nonlinear hysteretic behaviour. Earthq Eng & Struct Dyn 2013;42(13):1907–30. https://doi.org/10.1002/eqe.2304.
[44] Ruggieri S, Vukobratović V. The influence of torsion on acceleration demands in low-rise RC buildings. Bull Earthq Eng 2024;22(5):2433–68.
[45] Sagbas G, Sheikhi Garjan R, Sarikaya K, Deniz D. Field reconnaissance on seismic performance and functionality of Turkish industrial facilities affected by the 2023 Kahramanmaras earthquake sequence. Bull Earthq Eng 2024;22(1):227–54. https://doi.org/10.1007/s10518-023-01741-8.
[46] Saragoni GR, Hart GC. Simulation of artificial earthquakes. Earthq Eng & Struct Dyn 1973;2(3):249–67. https://doi.org/10.1002/eqe.4290020305.
[47] Singh MP, Moreschi LM, Suárez LE, Matheu EE. Seismic design forces. II: Flexible nonstructural components. J Struct Eng 2006;132(10):1533–42. https://doi.org/10.1061/(ASCE)0733-9445(2006)132:10(1533).
[48] Soong, T.T. and Grigoriu, M. (1993). Random vibration of mechanical and structural systems. Technical Report A, 93, 14690; NASA STI/Recon.
[49] Steib Pinto, F.J. (2011). Aceleración de piso en edificios de hormigón armado estructurados en base a muros sometidos a excitaciones sísmicas.
[50] Surana M, Singh Y, Lang DH. Effect of structural characteristics on damping modification factors for floor response spectra in RC buildings. Eng Struct 2021;242:112514.
[51] Taghavi S, Miranda MM. Response Assessment Of Nonstructural Building Elements. Pacific Earthquake Engineering Research Center; 2003.
[52] Zheng W, Chen J, Wang H, Tan P, Li J, Wang S. A novel damping adaptive pendulum isolation system for seismic resilience enhancement of continuous bridges. Eng Struct 2025;339:120465.